



Electronic structure of a single MoS₂ monolayer

Eugene S. Kadantsev^{a,b,*}, Pawel Hawrylak^b

^a Department of Chemistry, University of Ottawa, Ottawa, Canada K1N 6N5

^b Quantum Theory Group, Institute for Microstructural Sciences, National Research Council, Ottawa, Canada K1A 0R6

ARTICLE INFO

Article history:

Received 2 February 2012

Accepted 5 February 2012

by A.H. MacDonald

Available online 10 February 2012

Keywords:

A. Nanostructures

D. Electronic band structure

D. Optical properties

D. Electronic transport

ABSTRACT

The electronic structure of a single MoS₂ monolayer is investigated with all electron first-principles calculations based on Kohn–Sham Density Functional Theory and variational treatment of spin–orbital coupling. The topologies of the valence band maximum and conduction band minimum are explored over the whole Brillouin zone. The single MoS₂ monolayer is confirmed to be a direct band gap semiconductor. The projected density of states (PDOS) of a single monolayer is calculated and compared to that of bulk MoS₂. The effective masses and the orbital character of the band edges at high-symmetry points of the Brillouin zone are determined. The spin-splittings of the conduction band minimum (CBMIN) and valence band maximum (VBMAX) are calculated over the whole Brillouin zone. It is found that the maximum spin-splitting of VBMAX is attained at the **K** point of the Brillouin zone and is responsible for the experimentally observed splitting between the A₁ and B₁ excitons.

© 2012 Elsevier Ltd. All rights reserved.

1. Introduction

Molybdenum disulfide, MoS₂, is a “layered” transition metal dichalcogenide semiconductor [1] with an indirect band gap that has attracted considerable interest in connection with its catalytic and electronic properties [2–9]. The “layered” structure of MoS₂ is formed by a graphene-like hexagonal arrangement of Mo and S atoms stacked together to give S–Mo–S sandwiches coordinated in a triangular prismatic fashion (Fig. 1). The S–Mo–S sandwiches are bonded together by weak Van-der-Waals forces.

Recently, a number of groups [10,11] have reported emerging photoluminescence in MoS₂ thinned down to one S–Mo–S sandwich (single S–Mo–S monolayer). This photoluminescence was attributed to an indirect-to-direct band gap transition which stems from the sensitivity of the orbitals participating in the indirect transition to the “environment” [11]. It is hoped that further advances in fabrication of thin low-dimensional MoS₂ structures will pave the way to uncovering a plethora of exciting new physics [12–14] not encountered in graphene, due, for example, to the presence of transition-metal d-type orbitals in the valence and conduction bands. Therefore, there is considerable interest in understanding the electronic structure of thin MoS₂ films and, in particular, the electronic structure of a single MoS₂ monolayer.

In this work, we explore the properties of a S–Mo–S monolayer using Kohn–Sham Density Functional Theory [15–17]. The novelty of this work as compared to previous studies [18–23] is that we perform all electron calculations and include spin–orbital coupling variationally. The topologies of the valence band maximum (VBMAX) and conduction band minimum (CBMIN) are investigated over the whole Brillouin zone (BZ). We confirm with all electron calculations the indirect-to-direct band gap transition in a single S–Mo–S monolayer. We calculate the projected density of states (PDOS) in a single MoS₂ monolayer and compare it to the bulk PDOS. Parameters of the electronic structure such as the effective masses and the orbital populations of band edges are determined at several high-symmetry points of the Brillouin zone. Spin-splittings due to the loss of the inversion symmetry present in bulk MoS₂ in a single MoS₂ monolayer are explored for the CBMIN and VBMAX. This loss can result in a number of interesting physical effects such as the valley Hall effect [24] and valley-dependent optical selection rules [25].

All the calculations are carried out using the all-electron approach which combines Kohn–Sham Density Functional Theory (KS DFT) [15,16] in the local spin density approximation (LSDA) [17], variational treatment of spin–orbital coupling, and the Augmented Plane Wave plus Local Orbitals (APW + lo) representation [26,27]. Within this scheme, the core levels are treated fully relativistically and self-consistently in the spherical approximation, whereas the valence states are treated using a second-variational Hamiltonian [28,29]. The Perdew–Wang [30] parameterization of the correlation energy is employed. The EXCITING APW+lo program [31] is used. The local orbitals and linearization energies are taken from the program’s database. The pa-

* Corresponding author at: Department of Chemistry, University of Ottawa, Ottawa, Canada K1N 6N5.

E-mail addresses: ekadants@uottawa.ca, ekadants@yahoo.ca (E.S. Kadantsev).

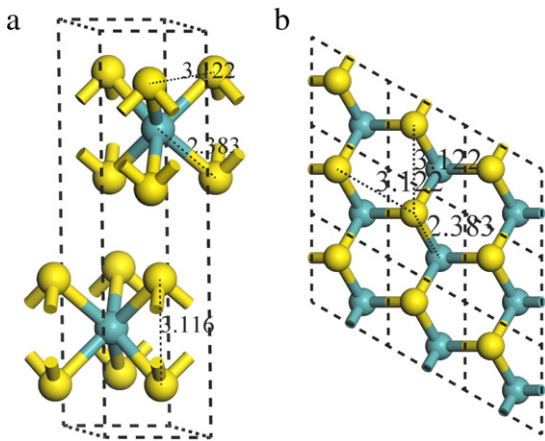


Fig. 1. Geometry of MoS₂. (Bulk: space group P6₃/mmc; $a = 3.122$ Å; $c = 11.986$ Å; and $z = 0.12$.) (a) Side view of a bulk unit cell (dashed line). The bulk unit cell has 2 Mo atoms (blue) and 4 S atoms (yellow). Each of the Mo atoms is coordinated to 6 S atoms in a triangular prismatic fashion (b) Top view of a graphene-like single S–Mo–S monolayer (3×3 unit cells). (For interpretation of the references to colour in this figure legend, the reader is referred to the web version of this article.)

parameter $R_{MT} \times K_{max}$ which determines the “size” of the plane wave basis set is set to 8.0. The Brillouin zone of a single S–Mo–S monolayer is sampled with $n \times n \times 1$ \mathbf{k} -points, where $n = 8 - 12$. The projected density of states is constructed with very accurate $31 \times 31 \times 1$ \mathbf{k} -point grids.

Atomic units $\hbar = e = m_e = 1$ are used throughout, unless otherwise specified.

2. Results

The MoS₂ bulk unit cell belongs to the space group P6₃/mmc and contains 6 atoms (2 Mo and 4 S). The structure is uniquely determined by the lattice constants a (hexagonal lattice constant) and c together with the internal displacement parameter $z = 0.12$. Our LSDA calculations yield $a = 3.122$ Å and $c = 11.986$ Å, in reasonable agreement with the experimental values of $a_{exp} = 3.16$ Å, $c_{exp} = 12.58$ Å. The larger than usual (5%) discrepancy in the lattice constant c is due to the well documented failure [32] of local and semi-local approximations for the exchange–correlation to describe the Van der Waals interactions. The S–S distances (3.116, 3.122 Å) are considerably larger than the bond length in the S₂ dimer (1.89 Å). The Mo–S bond distance is 2.383 Å (Fig. 1).

It is expected that the Mo 4d and S 3p atomic orbitals will play a decisive role in the properties of MoS₂. From atomic calculations, we find that the 3p S orbitals have a spatial extent that is very similar to that of the 4d Mo orbitals with expectation values of $\langle r \rangle = 1.10$ Å and $\langle r \rangle = 1.06$ Å, respectively. Taking into account that the separations of the Mo and “adjacent” S layers in the stacking direction are $0.5c = 6.0$ Å and $2zc = 2.9$ Å, respectively, one might expect that the energy levels dominated by the Mo d-orbitals (S p-orbitals) would be insensitive (sensitive) to the thickness of the MoS₂ films. In practice, this simple picture is further modified by the Mo d–S p orbital hybridization.

The band structure of the electron levels for a single MoS₂ monolayer along the lines connecting high-symmetry points of the Brillouin zone is shown in Fig. 2. In agreement with previous reports [10,11] the MoS₂ monolayer is a direct band gap semiconductor with a maximum of the valence and minimum of the conduction band (VBMAX/CBMIN) located at the \mathbf{K} \mathbf{k} -point of the BZ. From our calculations we find that the direct $\mathbf{K} \rightarrow \mathbf{K}$ gap is 1.79 eV and the indirect $\Gamma \rightarrow \mathbf{Q}$ gap is 2.03 eV. The computed band gap is in reasonable agreement with the experimentally measured

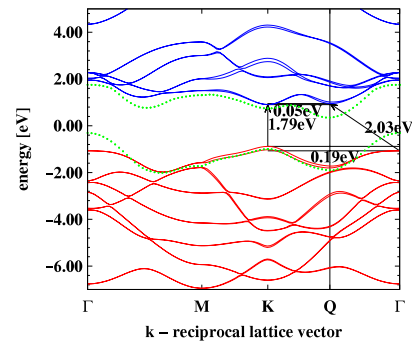


Fig. 2. The band structure of the electron levels for a single MoS₂ monolayer (red lines—valence band; blue lines—conduction band). A single MoS₂ monolayer is a direct band gap semiconductor with direct $\mathbf{K} \rightarrow \mathbf{K}$ and indirect $\Gamma \rightarrow \mathbf{Q}$ gaps (1.79 eV and 2.03 eV, respectively). VBMAX and CBMIN at the \mathbf{K} \mathbf{k} -point are located 0.19 eV above and 0.05 eV below the energies at the Γ and \mathbf{Q} \mathbf{k} -points, respectively. The green lines show the top (bottom) valence (conduction) bands in bulk MoS₂. Bulk MoS₂ is an indirect band gap semiconductor with direct $\mathbf{K} \rightarrow \mathbf{K}$ (1.74 eV) and indirect $\Gamma \rightarrow \mathbf{Q}$ (0.65 eV) gaps. (For interpretation of the references to colour in this figure legend, the reader is referred to the web version of this article.)

emission energy at 1.83–1.98 eV [10,11]. The \mathbf{Q} point of the BZ is located along the $\Gamma \rightarrow \mathbf{K}$ line $0.53|\Gamma\mathbf{K}|$ away from the Γ -point. We find that VBMAX and CBMIN at the \mathbf{K} \mathbf{k} -point are located 0.19 eV above and 0.05 eV below the energies at the Γ and \mathbf{Q} points, respectively (Fig. 2). Fig. 2 also shows the top of the valence band and bottom of the conduction band of bulk MoS₂ (green line). We find that bulk MoS₂ is an indirect bandgap semiconductor with the top of the valence band and bottom of the conduction band located at the Γ and \mathbf{Q} \mathbf{k} -points. The $\Gamma \rightarrow \mathbf{Q}$ and $\mathbf{K} \rightarrow \mathbf{K}$ gaps are 0.65 eV and 1.74 eV, respectively. We find that the LSDA strongly underestimates the experimental indirect band gap in bulk MoS₂, reported to be 1.29 eV (Ref. [10]). Overall, we find that the indirect $\Gamma \rightarrow \mathbf{Q}$ band gap is substantially destabilized in a single MoS₂ monolayer compared to that of the bulk (2.03 eV versus 0.65 eV), while the direct band gap remains unaffected (1.74 eV versus 1.79 eV).

We have further investigated VBMAX and CBMIN of a single MoS₂ monolayer by considering the topologies of these bands over the whole BZ (Fig. 3). We find that for the top valence band, the max and min values are attained at the Γ and \mathbf{K} -points and along the $\Gamma\mathbf{M}$ lines, respectively, with the global maximum located at the \mathbf{K} \mathbf{k} -point (Fig. 3(a)). For the bottom conduction band, the min values occur at \mathbf{K} \mathbf{k} -point and, approximately, half-way between Γ and \mathbf{K} points with global minimum located at \mathbf{K} (Fig. 3(b)). The max values are attained at the Γ and \mathbf{M} -points (Fig. 3(b)). Fig. 3 allows for some preliminary conclusions with respect to the anisotropy of the effective masses. In particular, the effective masses at the \mathbf{K} point are expected to be isotropic, whereas the conduction band effective mass at the \mathbf{Q} point is expected to be somewhat anisotropic.

We have determined the effective masses in a MoS₂ monolayer which allows for the calculation of exciton spectra and mobilities. The effective masses were determined in two ways. The first approach consisted in determination of the effective mass tensor using the \mathbf{k} -vector displacement of 0.025 a.u.^{−1} and the subsequent diagonalization of the effective mass tensor and determination of the principal values. The results of this approach were verified with a second calculation in which a local band structure was constructed in the neighborhood of the point of interest and a parabolic fit along different lines passing the point of interest was performed. The two sets of calculations agree very well.

The effective masses at the \mathbf{K} point are determined to be $m_e^* = 0.54$ for an electron in the CBMIN and $m_h^* = 0.44$ for a hole at the VBMAX. The directional dependences of the effective masses at the \mathbf{K} point are small (<0.01). The CBMIN effective mass at the

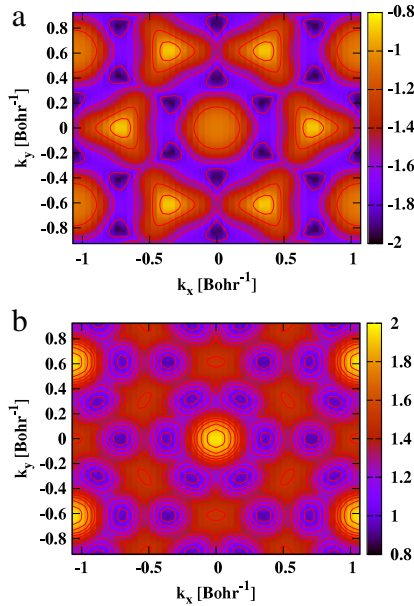


Fig. 3. Topology of the valence band maximum (VBMAX) and conduction band minimum (CBMIN) in a single MoS₂ monolayer. The colorscale bar unit is eV. The global maximum (minimum) of VBMAX (CBMIN) is located at the **K** **k**-point of the Brillouin zone.

Q point is directionally dependent and lies in the range 0.54–0.98. The directional dependence of the effective mass at the **Q** point is consistent with Fig. 3(b), where the isocontours around the **Q** point have an ellipsoidal shape. The VBMAX effective mass at the Γ point is found to be 5.25 and directionally independent.

It is interesting to note that the LSDA reproduces the direct gap $\mathbf{K} \rightarrow \mathbf{K}$ in a MoS₂ monolayer quite accurately (1.79 eV versus 1.83–1.98 eV) whereas, in agreement with a general trend, it strongly underestimates the indirect band gap in the bulk (0.65 eV versus 1.29 eV). To gain some insight into this situation, we performed a computational experiment in which two sheets of MoS₂ were pulled apart (or brought closer together) in the vertical (*c*) direction. The calculations were carried out in the supercell geometry with a large out-of-plane lattice constant $c = 60$ a.u. The initial atomic positions in the supercell were taken from the optimized bulk geometry. We then changed the separation between the two sheets and monitored the evolution of the direct $\mathbf{K} \rightarrow \mathbf{K}$ and indirect $\Gamma \rightarrow \mathbf{Q}$ band gaps. The evolutions of the band gaps as a function of the separation change from that of bulk are shown in Fig. 4. The zero change in separation corresponds to the bulk geometry. Fig. 4 shows that the direct $\mathbf{K} \rightarrow \mathbf{K}$ gap is insensitive to the separation between the two MoS₂ sheets and is very close in value to the direct band gap in a single MoS₂ monolayer. The value of the indirect band gap for two sheets of MoS₂ at the “bulk” geometry is 1.12 eV. This value is much larger than the indirect band gap in bulk MoS₂. As the two sheets are brought closer together (negative change in the separation on Fig. 4), the indirect band gap decreases dramatically. The negative change in separation region in Fig. 4 corresponds to stronger coupling between the two sheets and delocalization of the states involved in the indirect transition. It is most likely that the strong underestimation of the bulk indirect band gap is rooted in the well known pathologies of the local and semi-local exchange–correlation potentials such as the absence of discontinuities and the non-local nature of the true exchange–correlation potential ([33,34] and the references therein).

We have also calculated the projected density of states (PDOS) (Fig. 5) and performed orbital population analysis for the CBMIN

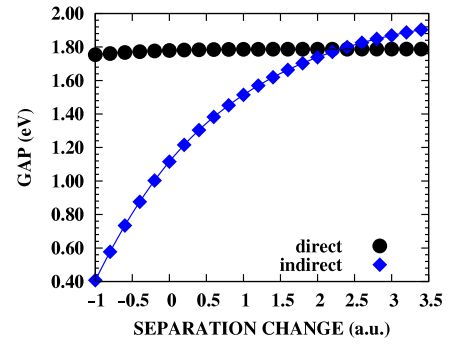


Fig. 4. The direct ($\mathbf{K} \rightarrow \mathbf{K}$) and indirect ($\Gamma \rightarrow \mathbf{Q}$) band gaps (eV) in two sheets of MoS₂ film as a function of the change in the separation (Bohr). The zero change in separation corresponds to the optimized bulk geometry. The direct band gap is insensitive to the separation, whereas the indirect band gap strongly depends on it.

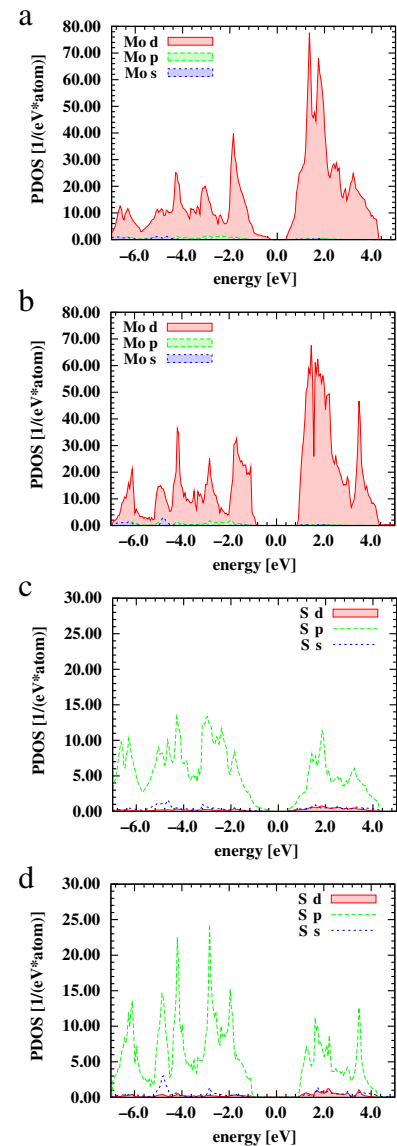


Fig. 5. The projected density of states (PDOS) in bulk and in a single MoS₂ monolayer.

and VBMAX band edges (Fig. 6) for a single MoS₂ monolayer. Within the APW+lo approach, the PDOS is calculated by weighting each contribution $\delta(E - E_{ik})$ in the density of states sum by a

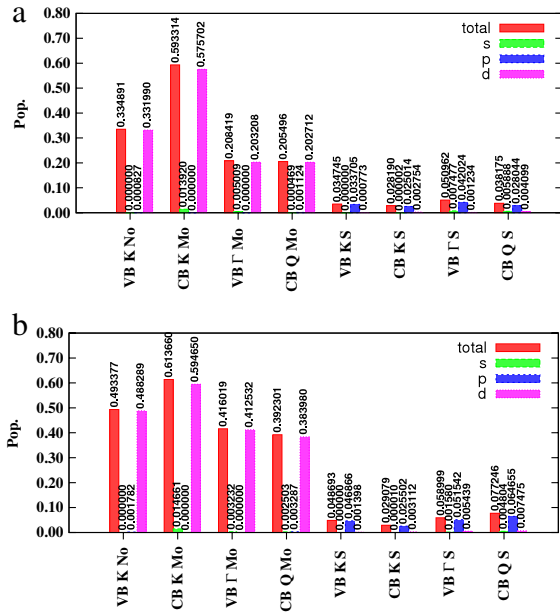


Fig. 6. Orbital populations of the conduction and valence bands at the **K**, **Q**, and Γ **k**-points of the BZ in bulk (a) and single monolayer (SM) MoS₂ (b).

state's projection (overlap) with a spherical harmonic $\langle \psi_{ik} | Y_{lm} \rangle$. The projection is calculated inside the muffin-tin sphere.

Our PDOS (Fig. 5) shows that the top of the valence (bottom of the conduction) band in bulk and single layer MoS₂ consists of Mo d- and S p-type contributions. The Mo PDOS for a single monolayer possesses edges that are characteristic to two-dimensional systems (for example, at the top of the valence band). It is interesting to note that these edges are less pronounced than those on the PDOS obtained without spin-orbital coupling (see, for example, Fig. 1 of Ref. [19]). Overall, the main features of the PDOS in the bulk and 2D systems look similar, although some smaller peaks appear and disappear. The PDOS in 2D is more spiky whereas the PDOS in bulk is more of a broad character.

Fig. 6 shows the orbital populations inside the muffin-tin spheres at high-symmetry points of the Brillouin zone. We find that both the conduction and the valence band orbitals at the **K** point are strongly localized on the metal ion (Mo). The strong localization of electrons at the **K**-point at Mo is consistent with the insensitivity of the direct **K** \rightarrow **K** band gap to the number of layers in MoS₂. We also find that the contribution of sulfur p-type states to the band edges is small compared to the Mo d-type contributions.

The relativistic interaction between the spin and angular momentum of the electron creates an internal magnetic field $\mathbf{B}_{\text{int}} = (1/2c^2)\nabla V(\mathbf{r}) \times \mathbf{p}$, where \mathbf{p} is the momentum and $V(\mathbf{r})$ is the crystal potential. This internal magnetic field couples with the electron spin contributing the $(1/2)\mathbf{B}_{\text{eff}} \cdot \vec{\sigma}$ term to the total Hamiltonian and can break down Kramer's degeneracy in systems without inversion symmetry, for example, zinc-blende semiconductors [35–38] as the two-fold degeneracy throughout the Brillouin zone is no longer required [35]. We will refer to this type of splitting as intrinsic (Dresselhaus) spin-splitting.

The bulk MoS₂ with two MoS₂ monolayers per unit cell possesses inversion symmetry. If one uses one of the Mo atoms as the center of inversion, the “inverted” sulfur atoms of the first MoS₂ monolayer will transform (with an application of a nonprimitive translation) into the sulfur atoms of the second MoS₂ monolayer. In the case of a single MoS₂ monolayer, the sulfur atoms will be transformed into an empty site. The transition from bulk MoS₂ to one MoS₂ monolayer removes the inversion symmetry (overall, the number of symmetry operations is reduced from 24 to 12) and

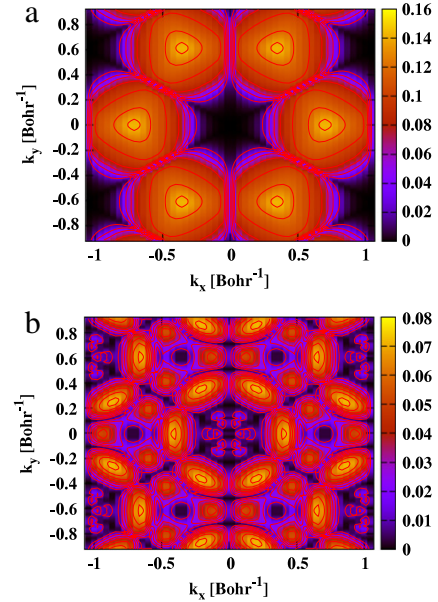


Fig. 7. Absolute magnitude of the intrinsic spin-splitting of the valence band maximum (VBMAX) and conduction band minimum (CBMIN) over the whole Brillouin zone. The colorscale bar unit is eV. The global maximum for VBMAX (CBMIN) is located at **K** (at the **Q** point half-way along the $\Gamma\mathbf{K}$ line). The regions with small (zero) spin-splittings are shown in dark (black) colors. The regions of the Brillouin zone with larger spin-splittings are shown with progressively lighter colors.

breaks down the Kramer's degeneracy in most of the Brillouin zone. We have therefore explored the intrinsic spin-splittings for the CBMIN and VBMAX bands in one MoS₂ monolayer over the whole Brillouin zone with the goal of determining the locations of the spin-splitting maxima and minima (Fig. 7).

We find that the VBMAX spin-splittings are very small in the vicinity of the Γ point (dark region in the center in Fig. 7(a)) and are exactly zero at the Γ point. The max spin-splitting for VBMAX is attained at the **K** point of the Brillouin zone and equals 145 meV (six bright regions in Fig. 7(a) arranged in a graphene-like lattice). We note that the spin-splitting maximum is located exactly on the line centered between the lines connecting neighboring minima at the Γ point.

The spin-splitting pattern for the CBMIN band is more complex with several local minima and maxima (Fig. 7(b)). We note that the CBMIN splittings are by a factor of 2 smaller than those for VBMAX. The max value of about 80 meV is attained in the neighborhood of the **Q** point which is located, approximately, half-way between the **K** and Γ points. There is also a smaller double maximum along the **KK** line which is separated by minima at the **K** and **M** points. The CBMIN spin-splittings are very small along the $\Gamma\mathbf{M}$ lines. We find that the CBMIN intrinsic spin splitting is exactly zero at the Γ point and is very small at the **K** point (3 meV).

We find that the value of the intrinsic spin-splitting at the **K** point of the Brillouin zone for the VBMAX is in very good agreement with the experimentally observed splitting between A_1 and B_1 excitons [11], probably due to the cancellation of the self-energy corrections. This good agreement further supports the conclusion that the photoluminescence in a single MoS₂ monolayer arises from the **K** to **K** transition.

3. Conclusions

We have investigated the electronic structure of a single MoS₂ monolayer. We find that a single MoS₂ monolayer is a direct **K** \rightarrow **K** bandgap semiconductor. Orbital population analysis indicates that the states responsible for the **K** \rightarrow **K** transition arise from

the Mo d-band and are strongly localized on the metal ion (Mo). We explored the topologies of the valence band maximum and the conduction band minimum over the whole Brillouin zone and determined local (and global) minima and maxima. The electron and hole effective masses at the \mathbf{K} point which allow for the calculation of the exciton spectra, mobility and density of states were calculated and found to be directionally independent. It was found that the maximum in the intrinsic spin-splitting of the VBMAX occurs at the \mathbf{K} \mathbf{k} -point and the magnitude of this splitting is in good agreement with the experimentally observed energy difference between A_1 and B_1 excitons. This good agreement further provides evidence that the photoluminescence of thin MoS_2 films originates from the \mathbf{K} to \mathbf{K} transition. Future work will focus on many-body corrections beyond Density Functional Theory to the optical properties of a single MoS_2 monolayer.

Acknowledgments

The authors thank D. Guclu, I. Ozfidan, and M. Potemski for discussions and the NRC-NSERC-BDC Nanotechnology program for financial support.

References

- [1] A.D. Yoffe, Chem. Soc. Rev. 5 (1976) 51.
- [2] L.S. Byskov, J.K. Nørskov, B.S. Clauden, H. Topsøe, J. Catalana 187 (2000) 109.
- [3] P. Raybaud, J. Hafner, G. Kresse, S. Kasztelan, H. Toulhoat, J. Catalana 189 (2000) 129.
- [4] M. Sun, A.E. Nelson, J. Adjaye, J. Catalana 233 (2005) 411.
- [5] N.M. Galea, E.S. Kadantsev, T. Ziegler, J. Phys. Chem. C 113 (2009) 193.
- [6] A. Vojvodic, B. Hinnemann, J.K. Nørskov, Phys. Rev. B 80 (2009) 125416.
- [7] T. Li, G. Galli, J. Phys. Chem. C 111 (2007) 16192.
- [8] E. Gourmelon, O. Lignier, H. Hadouda, G. Couturier, J.C. Bernede, J. Tedd, J. Pouzed, J. Salardenne, Sol. Energy Mater. Sol. Cells 46 (1997) 115.
- [9] M. Thomalla, H. Tributsch, J. Phys. Chem. B 110 (2006) 12167.
- [10] K.F. Mak, C. Lee, J. Hone, J. Shan, T.F. Heinz, Phys. Rev. Lett. 105 (2010) 136805.
- [11] A. Splendiani, L. Sun, Y. Zhang, T. Li, J. Kim, C.-Y. Chim, G. Galli, F. Wang, Nano Lett. 10 (2010) 1271.
- [12] B. Radisavljevic, A. Radenovic, J. Brivio, V. Giacometti, A. Kis, Nat. Nanotechnology 6 (2011) 147.
- [13] T. Korn, S. Heydrich, M. Hirmer, J. Schmutzler, C. Schuller, Appl. Phys. Lett. 99 (2011) 102109.
- [14] Y. Yoon, K. Ganapathi, S. Salahuddin, Nano Lett. 11 (2011) 3768.
- [15] P. Hohenberg, W. Kohn, Phys. Rev. 136 (1964) B864.
- [16] W. Kohn, L.J. Sham, Phys. Rev. 140 (1965) A1133.
- [17] U. von Barth, L. Hedin, J. Phys. C: Solid State Phys. 5 (1972) 1629.
- [18] L.F. Mattheiss, Phys. Rev. Lett. 30 (1973) 784.
- [19] S. Lebegue, O. Eriksson, Phys. Rev. B 79 (2009) 115409.
- [20] Y. Ding, Y. Wang, J. Ni, L. Shi, S. Shi, W. Tang, Physica B 406 (2011) 2254.
- [21] Y. Ma, Y. Dai, M. Guo, C. Niu, J. Lu, B. Huang, Phys. Chem. Chem. Phys. 13 (2011) 15546.
- [22] C. Ataca, S. Ciraci, J. Phys. Chem. C 115 (2011) 13303.
- [23] A. Kuc, N. Zibouche, T. Heine, Phys. Rev. B 83 (2011) 245213.
- [24] D. Xiao, W. Yao, Q. Niu, Phys. Rev. Lett. 99 (2007) 236809.
- [25] W. Yao, D. Xiao, Q. Niu, Phys. Rev. B 77 (2008) 235406.
- [26] E. Sjöstedt, L. Nordström, D.J. Singh, Solid State Commun. 114 (2000) 15.
- [27] G.K.H. Madsen, P. Blaha, K. Schwarz, E. Sjöstedt, L. Nordström, Phys. Rev. B 64 (2001) 195134.
- [28] D.D. Koelling, B.N. Harmon, J. Phys. C 10 (1977) 3107.
- [29] J. Kunes, P. Novak, R. Schmid, P. Blaha, K. Schwarz, Phys. Rev. B 64 (2001) 153102.
- [30] J.P. Perdew, Y. Wang, Phys. Rev. B 45 (1992) 13244.
- [31] Version 0.9.151. <http://exciting.sourceforge.net>.
- [32] S. Grimme, J. Antony, S. Ehrlich, H. Krieg, J. Chem. Phys. 132 (2010) 154104.
- [33] G. Onida, L. Reining, A. Rubio, Rev. Modern Phys. 74 (2002) 601.
- [34] R.W. Godby, Garcia-Gonzalez, Density Functional Theories and Self-Energy Approaches, in: Lecture Notes in Physics, vol. 620, Springer, Heidelberg, 2003.
- [35] G. Dresselhaus, Phys. Rev. 100 (1955) 580.
- [36] M. Cardona, N.E. Christensen, G. Fasol, Phys. Rev. B 38 (1988) 1806.
- [37] A.N. Chantis, N.E. Christensen, A. Svane, M. Cardona, Phys. Rev. B 81 (2010) 205205.
- [38] J.-W. Luo, G. Bester, A. Zunger, Phys. Rev. Lett. 102 (2009) 056405.